Carbon 215 (2023) 118486

Contents lists available at ScienceDirect

Carbon

journal homepage: www.elsevier.com/locate/carbon

1D selective confinement and diffusion of metal atoms on graphene

Srdjan Stavrić [a,b,c], Valeria Chesnyak [c,d], Simone del Puppo [c], Mirco Panighel [d], Giovanni Comelli [c,d], Cristina Africh [d], Željko Šljivančanin [b], Maria Peressi [c,e,*]

[a] Consiglio Nazionale delle Ricerche CNR-SPIN, c/o Università degli Studi "G. D'Annunzio", 66100 Chieti, Italy
[b] Vinča Institute of Nuclear Sciences - National Institute of the Republic of Serbia, University of Belgrade, P.O. Box 522, RS-11001 Belgrade, Serbia
[c] Physics Department, University of Trieste, via A. Valerio 2, 34127 Trieste, Italy
[d] CNR-IOM, Laboratorio TASC, S.S. 14 Km 163.5, Basovizza, 34149 Trieste, Italy
[e] ICSC - Italian Research Center on High Performance Computing, Big Data and Quantum Computing, Via Magnanelli 2, 40033 Casalecchio di Reno (BO), Italy

ARTICLE INFO

Keywords:
Graphene
Cobalt
Moiré
Numerical simulations
Scanning tunneling microscopy

ABSTRACT

The role of moiré graphene superstructures in favoring confined adsorption of different metal atoms is an intriguing problem not yet completely solved. Graphene (G) grown on Ni(100) forms a striped moiré pattern of valleys, where G approaches the nickel substrate and interacts with it rather strongly, and ridges, where G stays far away from the substrate and acts almost free-standing. Combining density functional theory (DFT) calculations and scanning-tunneling microscopy (STM) measurements, we show that this peculiar moiré constitutes a regular nanostructured template on a 2D support, confining in 1D trails single metal atoms and few atoms clusters. DFT calculations show that the confinement is selective and highly dependent on the atomic species, with some species preferring to adsorb on ridges and the other showing preference for valleys. Co and Au adsorbates, for instance, have opposite behavior, as predicted by DFT and observed by STM. The origin of such disparate behavior is traced back to the electrostatic interaction between the charged adsorbate and the nickel surface. Moreover, the selectivity is not restricted to the adsorption process only, but persists as adsorbate starts its diffusion, resulting in unidirectional mass transport on a continuous 2D support. These findings hold great promise for exploiting tailored nanostructured templates in a wide range of potential applications involving mass transport along element-specific routes.

1. Introduction

The rise of chemical vapor deposition (CVD) as the main method for synthesizing large samples of high-quality graphene (G) triggered intensive research on G interaction with closed-packed metal surfaces, such as the (111)/(0001) surfaces of fcc/hcp metals like Cu, Ni, Pt, Ir, Ru, Rh, that share the same lattice symmetry of G [1,2]. With the exception of the Ni(111) surface, in all other cases the lattice parameter mismatch between G and the underlying metallic surface causes the formation of superstructures, known as moiré patterns, with a hexagonal periodicity, where valleys (fcc and hcp regions) and mounds (atop regions) can be distinguished.

The G modulation introduces an anisotropy that can lead to preferential regions for adatom adsorption, diffusion and agglomeration. In the last fifteen years, many studies demonstrated that such systems can act as templates to grow small metal clusters with a narrow size distribution, for example Ir [3], Co [4], Dy [5] and Sm [6] on G/Ir(111) and Pt on both G/Ir(111) [7,8] and G/Ru(0001) [9]. The adsorption and adhesion energetics of supported nanoclusters are crucial for their surface reactivity [10] and sintering kinetics [11]. The moiré templates are potentially useful for catalytic applications as they keep the adsorbed atoms/clusters far apart from each other, thus preventing sintering phenomena that would quench their chemical activity.

Experiments and numerical simulations agree on the fact that small Ir and Pt clusters, as well as W and Re, occupy valleys (hcp-regions) on G/Ir(111) [3,8,12,13], but the preference for adsorption on valleys (or mounds) is not uniform among the elements of the periodic table, indicating possible different adsorption mechanisms [8,14–17]. In particular, it is found that alkali metal adatoms [14] and rare earth [17] on G/Ir(111) occupy the atop regions of the moiré, whereas transition metals preferentially adsorb on hcp regions [3]. Similar behavior of alkali metals and rare earths is attributed to a bond that is mainly ionic, with an electron transfer from the adatom to graphene. Knudsen [13] suggests that rehybridization from sp^2 to sp^3 bonding could be the key mechanism leading to preferential adsorption on valleys, as such rehybridization is only energetically favorable when C atoms sit directly above the substrate atoms. Other results are summarized in reviews of

* Corresponding author.
E-mail address: peressi@units.it (M. Peressi).

https://doi.org/10.1016/j.carbon.2023.118486
Received 29 June 2023; Received in revised form 19 September 2023; Accepted 25 September 2023
Available online 29 September 2023

the last decade [18–20] but it is impossible to infer a simple and general explanation for the observed selectivity that will allow to predict the preferred adsorption regions for different adatoms.

More complex moiré patterns occur when G is grown on metal substrates with non-hexagonal symmetry, such as (100)-oriented surfaces. Since (100) is one of the predominant orientations in polycrystalline Ni foils that are used to catalyze G synthesis, clarifying the structure and the properties of a G layer grown on this surface is also of application-oriented interest. Zou et al. demonstrated that G on Ni(100) can form either two-dimensional (2D) rhombic networks or quasi one-dimensional (1D) stripes and which one will be realized depends on the angular interface misorientation [21–23]. In stripe moiré patterns, G adopts parallel arrangements of valleys – the regions close to the Ni substrate with C atoms strongly interacting with the Ni atoms underneath – alternating with ridges where G is farther from the metal surface and interacts weakly with it. Besides obvious symmetry differences of 1D and 2D moiré patterns, the corrugation of the former is about 1 Å, much larger than of the later. This already may indicate that disparate regions of 1D moiré pattern display differences that are more pronounced than in 2D patterns.

In this paper, we combine density functional theory (DFT) calculations with scanning tunneling microscopy (STM) measurements to investigate the basic physical mechanism governing the preferential adsorption of different metal adatoms on valleys and ridges of stripe moiré G supported by Ni(100). The wide literature of G supported by Ni substrates, partially but not exhaustively cited in the present work, has proven that DFT gives a reliable description of this system. We find a clear selectivity that is ascribed to electrostatic effects connected to the direction of charge transfer between the adsorbate and G. As a proof of concept of our rationale, STM experiments show that Co single atoms and small clusters on top of G exhibit a clear preference for adsorption and diffusion on ridges. We thus prove that the stripy overstructure of G/Ni(100) constitutes a topographically 1D nanostructured template which provides a series of parallel race-tracks for mass transport, while remaining part of a continuous graphene sheet on a 2D support.

2. Methods

Computational details

DFT calculations were carried out using the Quantum ESPRESSO package [24,25]. Ni(100) is modeled by a three-layer slab in a 4 × 12 supercell as depicted in Figure S1 of Supporting Information. The DFT equilibrium bulk Ni lattice constant is 3.52 Å, a value widely accepted in literature; the G lattice constant of 2.46 Å enables matching the zig-zag chain of the carbon network with the [011] direction of the Ni(100) surface with a 1.2% strain [21]. The Brillouin zone was sampled with a 2 × 1 × 1 Γ-centered k-points mesh for structural relaxation and 4 × 2 × 1 mesh for self-consistent field calculations. The electronic exchange and correlation effects were described using the PBE functional [26] with Grimme DF-D2 van der Waals (vdW) corrections [27]. We chose this functional together with the Grimme DF-D2 correction because in a previous work [28] we verified that this computationally inexpensive approach reconciles most of the best results of the literature for G/Ni(111), and, in particular, gives a stable top-fcc configuration with substrate–overlayer distance and adsorption energy similar to those reported in Ref. [29] using a more sophisticated approach. Furthermore, the main physical aspects of Co adsorption on G/Ni(100) that we reported in our work are governed by the electrostatic Co-Ni interaction, which is not directly dependent on the level of description of the vdW interaction between G and Ni. The electron wave functions and density were expanded in plane waves basis sets with cutoff energies of 50 Ry and 300 Ry, respectively. All atoms but those from the bottom Ni layer were allowed to fully relax using the Broyden–Fletcher–Goldfarb–Shanno (BFGS) algorithm [30] until all the forces' components were less than 0.001 Ry/a_0 and the changes in the total energy for two consecutive cycles not greater than 10^{-4} Ry. Energy barriers for the diffusion processes of Co atoms were calculated employing the nudged elastic band (NEB) method [31,32] and the quasi-Newton Broyden optimization scheme. The Atomic Simulation Environment [33] and XCrySDen[34] packages together with our in-house python code were used for setting up and visualizing the obtained structures.

Experimental details

STM measurements were performed with a commercial Omicron low-temperature STM (LT-STM), operating at 77 K and $< 8\times10^{-11}$ mbar base pressure. The samples were prepared in the connected preparation chamber using the equipped sputter gun, gas line, a home-built evaporator and sample annealing stage. Ni(100) crystal was cleaned by at least three cycles of sputtering (15–20 min, 4 μA, 1 keV, $p_{Ar^+} = 1\times10^{-6}$ mbar) and annealing (10 min, 600 °C). Graphene was grown by CVD of ethylene at $p_{C2H4} = 3\times10^{-7}$ mbar while keeping the sample at 580 °C for 2 h. Similar amounts of Co and Au (<0.05 ML) were separately evaporated on the G/Ni(100) surface kept at 77 K. The STM images were processed with the Gwyddion software [35].

3. Results and discussion

Graphene stripe moiré on Ni(100): ridges and valleys

First of all, the wavy structure of stripe moiré in G/Ni(100) suggests a possible role of the curvature and of the strain on the adsorption and diffusion of adatoms. Indeed, there is a wide literature proposing to tailor the adsorption energetics of a G sheet by rippling or straining it.

Many theoretical/computational works predicted an enhancement of chemical activity in highly corrugated G [36,37]. Interestingly, the preference for adsorption on regions of positive or negative curvature cannot be generalized. Very recently, Banerjee et al. [38,39] showed that covalent and noncovalent interactions provide opposite molecular migration directions for adsorbates on a sinusoidally curved graphene. Imam et al. [40], studying highly corrugated G on Ir(001), showed that there is a critical curvature beyond which the reactivity of G increases remarkably. On the basis of this study, we inspected the role of curvature in G/Ni(100). We focus here only on those properties of the wavy G that are relevant for the present investigation and we address the reader to Ref. [21] for other details. We label the graphene C atoms on valleys/ridges as C_V/C_R, respectively. The stripe moiré has a period of 15 Å and an amplitude of about 1 Å (Fig. 1a), with wider valleys (V) and narrower and more curved ridges (R). Therefore, C atoms are not evenly distributed, with approximately 70% (30%) of them belonging to V (R) regions. To quantify the local curvature of G, we adopted the definition from Ref. [41], where the displacement d of a C atom normal to the plane defined by its three nearest neighbors is used as a measure. Using this measure, the G curvature at ridges does not exceed 0.08 Å , which is almost half of the critical value reported in Ref. [40]. Therefore, we conclude that curvature alone has no influence on the reactivity of G on Ni(100) and that the interaction with the metallic substrate must play a major role.

A comment is in order concerning the possible strain effects. Ref. [42] shows that on flat free-standing graphene a biaxial elongating strain as small as 1% strengthens the adsorption of some transition metal (TM) adatoms and associates the corresponding drop in energy with a smaller saturation of the C–C bonds under strain. Indeed, in our case the strain is similar: in the stripe moiré configuration the carbon–carbon bonds are on average 1.44 Å long, with a minimum/maximum length of 1.42/1.46 Å on ridges/valleys (see Figure S15 in Ref. [21]), and thus on the basis of this argument the adsorption of adatoms should be always favored on valleys rather than on ridges. In our case, instead, the behavior is dominated by the G/substrate interaction (present both in valleys and ridges and both in stretched and in

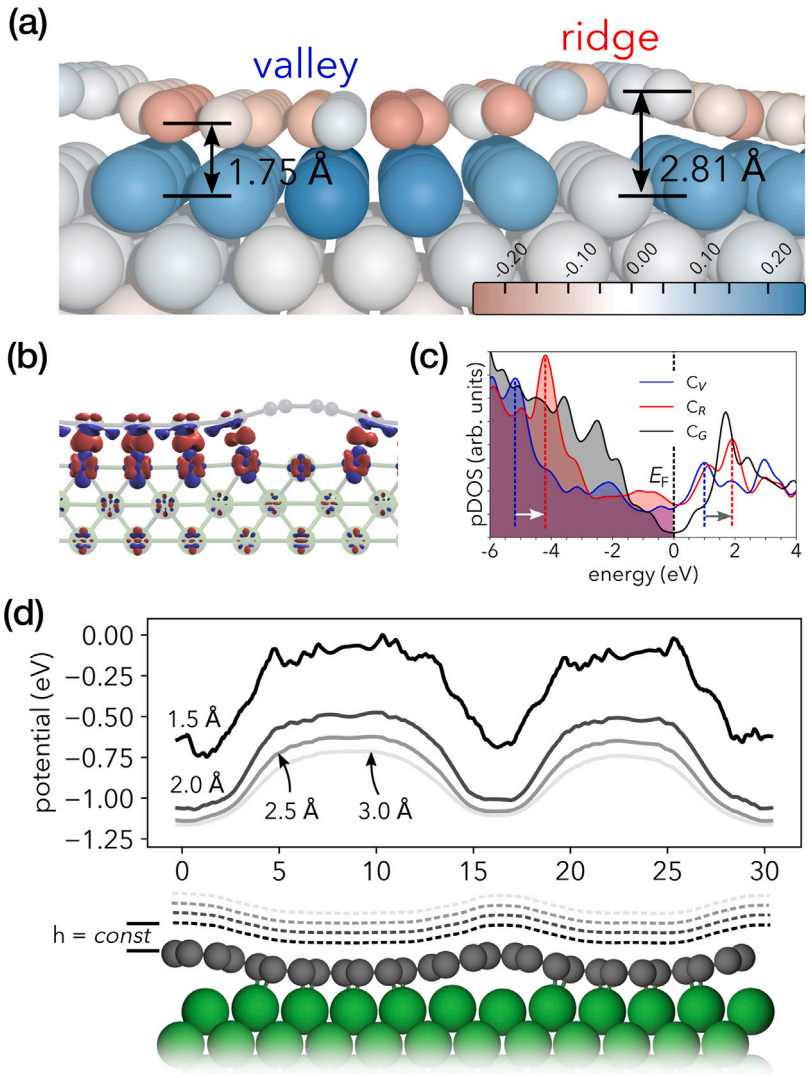

Fig. 1. (a) G/Ni(100) structure with atoms (large spheres: Ni; small spheres: C) colored according to their charges. Red (blue) color denotes negative (positive) total (ionic and electronic) charge (expressed in $|e|$). (b) Electronic charge density induced upon G adsorption on Ni(100): red (blue) color denotes regions with abundance (scarcity) of electrons. The plotted charge isocontour is for 0.005 e/a_0^3. (c) DOS projected on 2p orbitals of C atoms on valleys (C_V) and ridges (C_R) and of free standing G (C_G) for comparison. (d) Electrostatic potential profiles generated by G/Ni(100) calculated along lines parallel to the corrugated G at different heights (dashed lines); each value is obtained by averaging the potential along the direction parallel to the moiré stripes. (For interpretation of the references to color in this figure legend, the reader is referred to the web version of this article.)

compressed G regions [43]) and thus different elements prefer different adsorption regions, as will be extensively discussed in the subsection "Electrostatically-driven selective adsorption of adatoms on valleys and ridges".

A closer inspection of C_R and C_V atoms shows that the former are loosely bound to Ni(100) as they are sitting 2.81 Å above the surface, whereas the latter are only 1.75 Å above, facilitating the overlap between the C-2p_z and Ni-3d_{z^2} orbitals. Thus, the two disparate G regions are affected by the substrate to much different extent, as observed in Ref. [21] and shown in Fig. 1b by the plot of the charge density rearrangement induced upon G adsorption. Actually, the C_V atoms interact with Ni(100) even more than C atoms do with Ni(111), which is a substrate well known for interacting strongly with G [28,44]. Firstly, C_V atoms are about 0.35 Å closer to Ni(100) than C atoms are to Ni(111). Secondly, if we take the average binding energy (E_b) of G on Ni(100) which is $E_b = 0.18$ eV per C atom and assume that roughly only the valleys are contributing to binding, the estimate of the effective E_b for C_V rises up to 0.25 eV per atom. For comparison, the E_b of G on Ni(111) is 0.17 eV per C atom[28].

The degree of hybridization of C-2p orbitals from different regions can be inspected from the projected density of states (pDOS) shown in Fig. 1c. The Dirac cone in G disappears, due to the hybridization with the Ni-3d states, as already shown by Sala et al. [43] both by the calculated electronic bands (Fig. S5 of the Supporting Information of Ref. [43]) and by the dI/dV intensity curves (Fig. 2 of Ref. [43]), which in valleys and ridges are clearly different with respect to the regions where G is almost free-standing ("pseudo-ribbon"). Although the hybridization destroys the peculiar features of the G electronic structure around the Fermi energy, the relative positions of the most pronounced pDOS peaks show that C_V/C_R electronic states are shifted by roughly 1 eV, as indicated by the arrows in Fig. 1c. The shift comes from the n-doping of G on Ni(100) [43], as the majority of electrons transferred from the Ni substrate to G are distributed among the C_V atoms. This charge picture is supported by the plot of the induced charge density which shows no charge transfer between the C_R atoms and the Ni substrate (Fig. 1b).

To quantify the charge transfer, we calculated the Bader charges around atoms [45]. Fig. 1a shows the spatial distribution of the electronic charge: a detailed analysis indicates that on average Ni atoms below the valleys donate 0.16 electrons to G, with the middle row (darkest shade of blue) contributing the most. The charges on Ni atoms

from different rows are not exactly the same, which is a consequence of the gradual shift of G registry across the stripe. On the other side, charges on C_V atoms show higher non-uniformity, fluctuating along the valley with an average Bader charge of $-0.08e$ per C_V atom. Bader analysis clearly distinguishes the row of Ni atoms below the ridge (large gray spheres) from the others. Apart from charge neutrality, these Ni atoms are pushed downwards by 0.2 Å due to reorientation of neighboring $3d$ orbitals (Fig. 1b).

The modulation of the G structure and even more of the G–substrate interaction, that is alternating between strong (on V) and weak (on R), generates a pronounced modulation of the effective electrostatic potential offered to possible adsorbates, with narrow minima and wider maxima in correspondence to the width of R and V regions (Fig. 1d). We averaged the electrostatic potential along the [011] direction and plotted it along parallel paths (l_h) that follow the shape of ripples at different heights h from G. Evidently, the electrostatic potential is deeper above the ridges, with the R/V potential difference ranging between the 0.6 eV at $h = 1.50$ Å and 0.4 eV at $h = 3.00$ Å. Reasonably, as the height increases the potential is becoming flatter and the difference between V and R is gradually decreasing, but in the height interval that is relevant for the adsorption of different atomic species (between 1.5 Å and 3.0 Å) the R/V difference is substantial and has undoubtedly the power to drastically alter the bonding and the mobility of adatoms on the G surface. Therefore, we expect that adatoms that are positively charged upon their adsorption on graphene will sit on ridges whereas those that are negatively charged will prefer valleys.

Distribution of Co adatoms and clusters: DFT calculations

As a first test case we calculated explicitly the adsorption on V and R of individual Co atoms and small clusters, which are very interesting for their magnetic properties.

In general, for a cluster A_n (A is the atomic species, n the number of atoms in the cluster) we define the adsorption energy as

$$E_{\text{ads}} = \frac{1}{n}\left(E_{A_n/\text{substrate}} - nE_A - E_{\text{substrate}}\right) \quad (1)$$

where the three total energies refer to the entire system ($E_{A_n/\text{substrate}}$), the isolated atom (E_A), and the bare substrate ($E_{\text{substrate}}$), respectively. Eq. (1) is similar to Eq. (1) of Ref. [46], apart from a change of sign (there we defined a "binding energy" instead of an "adsorption energy"). We thus calculate the adsorption energy of individual Co atom at high symmetry sites on valleys and ridges. Co adsorbs on the center of hexagon (H-site) on the free-standing G sheet [47–49] but the presence of the metallic substrate underneath G can alter the favorable adsorption site [50]. On G/Ni(100) we found that hollow sites stay the favorable ones. Yet, at variance with the free-standing G case, on G/Ni(100) we distinguish two types of H sites – those on ridges (H_R) and those on valleys (H_V), where for a single Co adatom we obtain very different E_{ads} of −1.50 and −1.01 eV for H_R/H_V, respectively (Fig. 2). Such a huge difference can be explained with the help of charge transfer analysis.

From the Bader analysis we estimate a charge transfer of 0.48/0.55 electrons from Co adatoms to the surface at H_V/H_R sites (0.70/0.72 using the Löwdin method). Therefore, Co adatoms donate electrons to G emerging from the adsorption as positive ions. Although both the charge and the distance from G are very similar for the H_V and H_R sites, the distance from Co to the nickel support differs substantially in the two cases, being 0.73 Å higher at H_R. Larger Co-Ni distance combined with less positively charged Ni atoms underneath (Ni row directly below the ridge is charge neutral) result in much weaker repulsion between the Co adatoms and the Ni surface below the ridge. Hence, the adsorption energy at H_R is more negative than at H_V.

In order to verify if the predicted behavior is strictly related to the chemical species involved and not to the fact that we are considering single adatoms, we inspect the adsorption of Co clusters. Due to the computational demands we restrict the discussion to clusters with up to five atoms. In Fig. 2a the adsorption energy on both V (in blue) and R (in red) is plotted as a function of the number of Co atoms in the cluster. For clusters of more than 3 atoms both 2D and 3D arrangements are considered. The Co clusters on valleys and ridges have very similar shape and in general are reminiscent of equiatomic Co clusters on free-standing G [51], displaying a clear preference for 3D geometries already from tetramers. This is not surprising because Co, as a transition metal with a high cohesive energy, tends to build structures with a high coordination, similar to other TMs [52]. Co crystallizes in a hcp structure and even at surfaces where it binds more strongly than on G it prefers to form the hcp-like clumps [46]. On G/Ni(100), E_{ads} for clusters on ridge is always higher than on valley with their difference being nearly constant across the cluster sizes, which is a consequence of stronger electrostatic repulsion with the Ni surface on valley. On the basis of our DFT simulations, we expect Co single atoms and small clusters to selectively adsorb on ridges due to electrostatic effects.

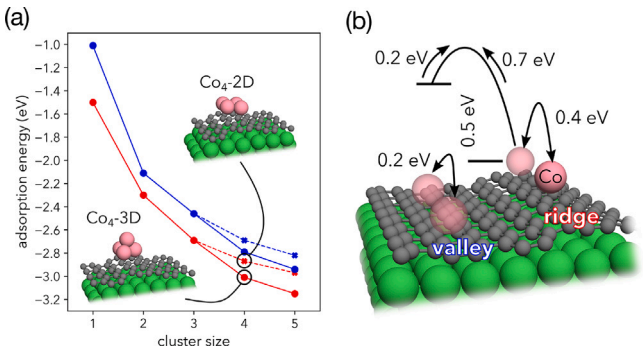

Fig. 2. (a) Adsorption energy of small Co clusters on valleys (blue) and ridges (red) (all the structures are shown in Figure S2 of Supporting information). Dashed lines connect the adsorption energies of 2D clusters that are less stable than their 3D counterparts (closed circles connected by solid lines). (b) Different diffusion paths for Co adatom on G/Ni(100) and the corresponding diffusion barriers calculated by the NEB method. (For interpretation of the references to color in this figure legend, the reader is referred to the web version of this article.)

Details on the magnetism of adsorbed Co atoms and clusters calculated by DFT are reported in Supporting Information (Figure S2).

Distribution of Co adatoms and clusters: experimental evidence

To verify our DFT predictions we performed low-temperature STM experiments. A small coverage (< 5%) of Co was deposited on G grown on a Ni(100) single crystal kept at 77 K. Although a sizable fraction of big clusters was always present – most probably as a consequence of the sample transfer process from the preparation chamber into the STM, when cooling was interrupted – a sufficient number of small clusters and single adatoms was detected for a meaningful analysis.

In Fig. 3a, single adatoms, small clusters (1.5 nm/0.25 nm apparent full-width-at-half-maximum (FWHM)/height), and large aggregations (2.5 nm/0.6 nm apparent FWHM/height) of Co are highlighted in pink/red/green, respectively. It is evident that all Co nanostructures are centered on ridges, irrespective of their size, even when it exceeds the width of a single ridge, confirming the expectations based on the DFT results. It has to be noted that the size of the largest clusters here is limited to the nanometer scale, at variance with 3D Co agglomerates on different substrates.[4,53]

Attribution of these structures to graphene protrusions above intercalated Co atoms or clusters can be excluded since we verified that the intercalation process starts at much higher temperatures (~250-300 °C).

For the sake of comparison, we investigated the behavior of another metal displaying different electronic properties. In particular, we

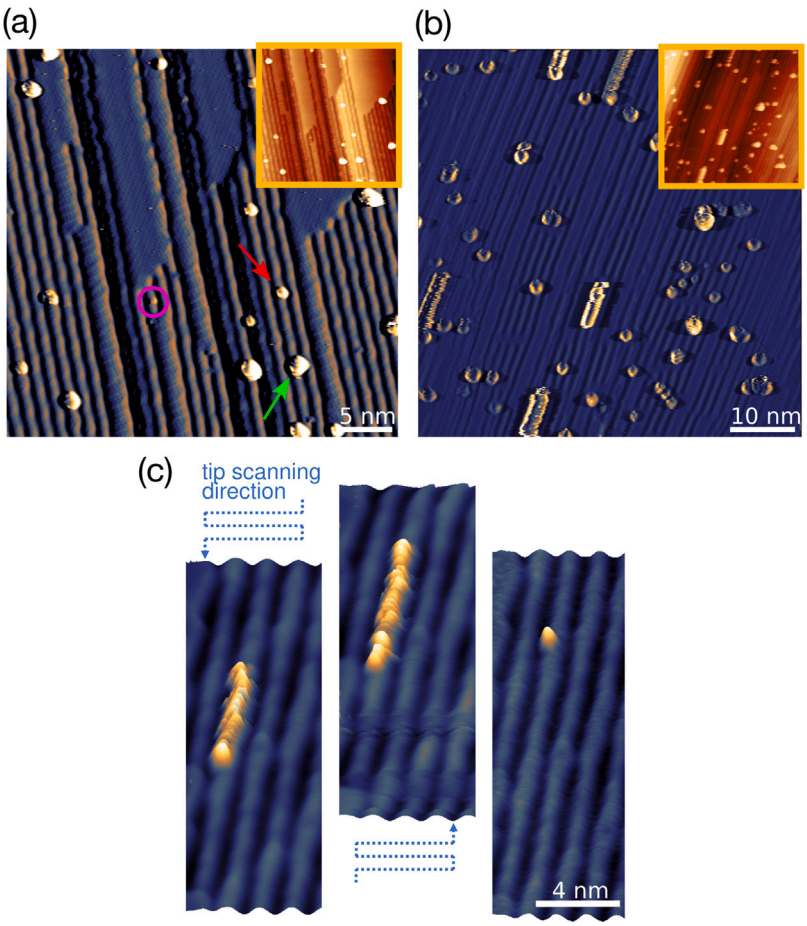

Fig. 3. STM images of Co clusters and adatoms on G/Ni(100). (a) A large-scale tunneling current image (measured point-by-point immediately before the feedback action) displaying both large (green arrow) and small (red arrow) clusters, as well as an adatom (pink circle) situated on the ridge. The apparent asymmetric shape of the clusters, with a dark shadow on the left and a larger extension on the right, is an artifact related to the feedback response time. The corresponding topographic image is shown in the inset. (b) STM image capturing the tip-induced movement of Co clusters along the ridges. The tunneling current channels while scanning forward and backward are averaged here to reduce the artifacts created by the feedback response to the fuzzy diffusing atoms. The corresponding topographic image is shown in the inset. (c) Tip-induced movement of a Co adatom along the ridge for two different scanning direction. The last panel shows the adatom at rest. Scanning parameters: (a) $V = -1.5\,\mathrm{V}$, $I = 0.2\,\mathrm{nA}$, (b) $V = -1.7\,\mathrm{V}$, $I = 0.2\,\mathrm{nA}$, (c) $V = -1.5\,\mathrm{V}$, $I = 0.2\,\mathrm{nA}$. (For interpretation of the references to color in this figure legend, the reader is referred to the web version of this article.)

performed a new experiment, evaporating on G/Ni(100) the more electronegative metal Au, with approximately the same coverage of Co. As shown in Figure S3, Au forms small clusters too, but, at variance with Co, they preferably reside at the valley sites. More precisely, statistical analysis of our STM images indicates that ~60% of the Au structures are residing strictly at the valleys, ~15% at the ridges and the remaining ~25% in between the two areas. The strikingly different behavior of Co and Au can be rationalized considering the electrostatically-driven adsorption of these adatoms, as described in detail in the next section.

Electrostatically-driven selective adsorption of adatoms on valleys and ridges

To further investigate the role of the electrostatic interaction between the adatoms and the nickel surface underneath G in dictating the preferential adsorption regions, we extend the DFT analysis to other selected chemical species. We take into account adatoms with qualitatively different charge transfer by considering highly electronegative elements (F, Au), metals that stay nearly neutral upon adsorption on G (Cu, Zn), as well as elements that donate electrons to G (the alkali element Li and TMs Ti, Ni) [54].

For all the inspected elements we consider the adsorption on R and V and calculate the total charges of the adatom (q_R and q_V) and the adsorption energy (E_R and E_V). In Fig. 4 we plot the correlation between the average total charge of the adatom $q = (q_R + q_V)/2$ as obtained from Löwdin analysis and the difference in adsorption energies $\Delta E = E_R - E_V$ on R and V. At variance with the adsorption energy, the total charge does not change much between R and V. Qualitative differences in charge transfer of the least and the most electronegative elements, Li and F, places them on the two opposite sides of the graph; TMs are on the far right, scattered around Li (square symbols), whereas tiny charge transfer reserves a place in the middle of the graph for Zn and Cu. Between neutral Zn and highly negative F alone lies moderately negative Au. The black dashed line in Fig. 4 serves as a guide to the eye but its linearity is a clear fingerprint that the correlation between the charge transfer and different stability of adsorbates on R and V is due to the electrostatic potential energy difference between the two regions. Alternative plot with charges calculated with Bader analysis is provided in Figure S4 of the Supporting Information. In a nutshell, the electrostatic potential is lower at the ridge and thus positive adatoms are attracted there, while the opposite stands for the atoms that carry negative charge upon the adsorption. In this way the electrostatic potential above the buckled G selectively sorts adatoms between the valleys and the ridges according to their charge.

DFT predictions provide a convincing explanation not only to the observed preference of Co/Au adsorption for R/V sites, but also to the fact that for Au this tendency is not as strong as for Co. This is indeed consistent with the fact that the calculated energy difference between R and V sites for Co is 0.5 eV, whereas for Au the V sites are favored by only 0.2 eV. Moreover, the diffusion barrier for Au along V and R is similar, about 0.2 eV. For these reasons some Au atoms and clusters are found at less favorable sites.

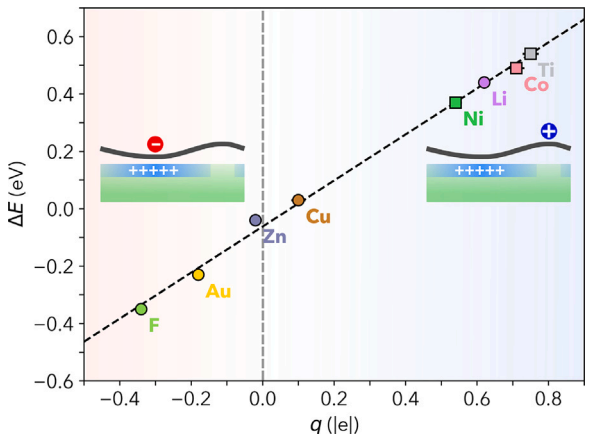

Fig. 4. The dependence of the adsorption energy difference ΔE on adatom total charge q, averaged over ridge and valley. Charges are obtained with Löwdin analysis. Short dashes sticking out behind the symbols represent the difference Δq in adatom charges on R and V (obviously, if Δq is smaller than the apparent width of the symbol the dashes are not visible).

Ridges as race tracks for Co adatoms diffusion

STM experiments on Co single atoms and small clusters indicate that the selectivity in adsorption is complemented by a confinement effect. As shown in Fig. 3b, they are easily moved on the surface upon interaction with the STM tip, thus artificially appearing as elongated stripy features. An example of such tip-induced movement for a single Co adatom is presented in Fig. 3c, with the image on the right showing the adatom (finally) at rest. Similar manipulations of adsorbates by the STM tip are well known [55,56], but what is remarkable here is the direction of the diffusion: the Co adatom and clusters always move parallel to the ridge irrespective of the tip sweeping direction. The preference of Co structures for ridges is a clear indication of a strong attractive interaction with the ridge and of a high barrier for the diffusion towards the valley.

Incidentally, the fact that it is possible to manipulate Co atoms and aggregates by the STM tip confirms that they are adsorbed above the G layer and not intercalated below it. In the latter case, manipulation would not be possible: a tip-induced movement of Co on Ni(100) is by itself unlikely since the calculated diffusion barrier of Co on Ni is about 0.8 eV [46] and the cover by graphene would make the process even more difficult.

To reveal how the stripes affect the mobility of Co atoms on G, we used the NEB method to calculate the barriers for their diffusion along valleys, ridges, and between the two regions (Fig. 2b). The energy barrier for diffusion along the ridge/valley is 0.4 eV/0.2 eV. The lower barrier for the diffusion along the valley is most likely the consequence of the repulsion between the positively charged adatom and the positively charged nickel surface underneath. The barrier for the diffusion from the valley to the ridge along a H–bridge–H path is again only 0.2 eV. Such small value suggests that adatoms easily reach the ridge and stay there, as the energy barrier to diffuse back to the valley is as high as 0.7 eV. These results demonstrate that the G stripes lead to anisotropy in Co diffusion, with a clear tendency of adatoms to move towards the ridges and along them. Moreover, this diffusion is even easier than on a flat free standing G, where the barrier along a H–bridge–H path is about 0.5 eV. Thanks to the regular morphology of stripe moiré, which extends in parallel stripes on areas of hundreds of nanometers up to micrometer size, the observed behavior suggests in principle the possibility of inducing at low temperature a long-range 1D mass transport embedded in a 2D matrix.

4. Conclusions

In conclusion, DFT calculations reveal that the stripe moiré pattern formed by G on Ni(100) leads to a selective adsorption of single atoms and small clusters on ridges or valleys. The mechanism underlying this behavior is traced back to electrostatic effects following a simple rule: positively charged adatoms, which donate electrons to G, adsorb on ridges, whereas negatively charged ones, which take electrons from G, prefer to stay on valleys. STM experiments confirm that Co single atoms and small clusters that donate electrons to G sit exclusively on ridges, whereas Au adsorbates, which take electrons from G, prefer valleys. The bond predicted by DFT between the single Co adatoms and G is 0.5 eV stronger on ridges than on valleys. This pronounced adsorption energy difference is due to the repulsive electrostatic interaction between the positively charged Co adatoms and the Ni atoms from the surface; at the buckled G sheet, Co adatoms tend to maximize the distance from the Ni surface and thus adsorb on the ridges, which are 1 Å farther from the surface than the valleys. Combined STM measurements and DFT calculations prove that the ridges confine Co adatoms and small clusters, due to an energy barrier of only 0.2 eV for the Co diffusion from the valley to the ridge and 0.7 eV for diffusion in the opposite direction, and a 0.4 eV barrier for diffusion along the ridge. As a consequence, the stripe moiré cannot constitute a template to keep adatoms and their aggregates into a fixed position, but instead opens new intriguing possibilities, since it allows 1D confinement and directional diffusion, with mass transport. At variance with Ref. [57], where the directional motion of the Co adsorbate is obtained on nanoribbons grown on a substrate, here the peculiar nanostructure of the stripe moiré naturally provides several parallel trails in a specific direction in micrometer sized areas. Our results open the way to future research efforts were the intriguing characteristic of graphene moiré are exploited with the aim of creating element specific surface paths for mass transport processes tailored at the single atom level.

CRediT authorship contribution statement

Srdjan Stavrić: Conceived the simulations, Performed and analyzed the simulations, Manuscript writing. **Valeria Chesnyak:** Conceived the experiments, Performed the experiments, Analyzed the experimental data, Manuscript writing. **Simone del Puppo:** Performed and analyzed the simulations, Manuscript writing. **Mirco Panighel:** Conceived the experiments, Performed the experiments, analyzed the experimental data, Manuscript writing. **Giovanni Comelli:** Manuscript writing. **Cristina Africh:** Conceived the experiments, Manuscript writing. **Željko Šljivančanin:** Manuscript writing. **Maria Peressi:** Conceived the simulations, Manuscript writing.

Declaration of competing interest

The authors declare that they have no known competing financial interests or personal relationships that could have appeared to influence the work reported in this paper.

Acknowledgments

We acknowledge financial support from MAECI, Italy (Executive Programme with Serbia 2019–2021) and MIUR, Italy (PRIN Bando 2017 – grants n. 2017KFY7XF and n. 2017NYPHN8). M.Pe. acknowledges support from Fondazione ICSC - "Italian Research Center on High-Performance Computing, Big Data and Quantum Computing" - Spoke 7, Materials and Molecular Sciences - National Recovery and Resilience Plan (PNRR) - funded by MUR Missione 4 - Componente 2 - Investimento 1.4 - Next Generation EU (NGEU), Italy. Computational resources have been obtained from CINECA through the ISCRA initiative and the agreement with the University of Trieste. Ž. Š. acknowledges support from the Serbian Academy of Sciences and Arts,

Serbia under grant F-18. We gratefully acknowledge Cinzia Di Giorgio and Alessandro Sala for their help with the experiments related to adsorption of Au clusters.

All authors have approved the final version of the manuscript.

Appendix A. Supplementary data

Supplementary material related to this article can be found online at https://doi.org/10.1016/j.carbon.2023.118486.

- Detailed description of the simulation supercell; Figure S1
- DFT magnetic moments of adsorbed Co atom and clusters; Figure S2
- STM images of adsorbed Au atoms and clusters; Figure S3
- Detailed description of the DFT results concerning the adsorption of different atomic species on valleys and ridges. Data shown in Fig. 4 of the Main Text is listed in Table S1; Figure S4 is an alternative version of Fig. 4 with charges obtained from Bader analysis.

References

[1] J. Wintterlin, M.-L. Bocquet, Graphene on metal surfaces, Surf. Sci. 603 (2009) 1841–1852.
[2] M.D. Jiménez-Sánchez, C. Romero-Muñiz, P. Pou, R. Pérez, J.M. Gómez-Rodríguez, Graphene on Rh(111): A template for growing ordered arrays of metal nanoparticles with different periodicities, Carbon 173 (2021) 1073–1081.
[3] A.T. N'Diaye, S. Bleikamp, P.J. Feibelman, T. Michely, Two-dimensional Ir cluster lattice on a graphene moiré on Ir(111), Phys. Rev. Lett. 97 (2006) 215501.
[4] C. Vo-Van, S. Schumacher, J. Coraux, V. Sessi, O. Fruchart, N.B. Brookes, P. Ohresser, T. Michely, Magnetism of cobalt nanoclusters on graphene on iridium, Appl. Phys. Lett. 99 (2011) 142504.
[5] R. Baltic, M. Pivetta, F. Donati, C. Wäckerlin, A. Singha, J. Dreiser, S. Rusponi, H. Brune, Superlattice of single atom magnets on graphene, Nano Lett. 16 (2016) 7610–7615.
[6] D. Mousadakos, M. Pivetta, H. Brune, S. Rusponi, Sm cluster superlattice on graphene/Ir(111), New J. Phys. 19 (2017) 123021.
[7] S. Linas, F. Jean, T. Zhou, C. Albin, G. Renaud, L. Bardotti, F. Tournus, Moiré induced organization of size-selected Pt clusters soft landed on epitaxial graphene, Sci. Rep. 5 (2015) 1–9.
[8] N. Podda, M. Corva, F. Mohamed, Z. Feng, C. Dri, F. Dvorák, V. Matolin, G. Comelli, M. Peressi, E. Vesselli, Experimental and theoretical investigation of the restructuring process induced by CO at near ambient pressure: Pt nanoclusters on graphene/Ir(111), ACS Nano 11 (2017) 1041–1053.
[9] Y. Pan, M. Gao, L. Huang, F. Liu, H.-J. Gao, Directed self-assembly of monodispersed platinum nanoclusters on graphene moiré template, Appl. Phys. Lett. 95 (2009).
[10] J. Bord, B. Kirchhoff, M. Baldofski, C. Jung, T. Jacob, An atomistic view of platinum cluster growth on pristine and defective graphene supports, Small 19 (2023) 2207484.
[11] K. Zhao, N. Janulaitis, J.R. Rumptz, C.T. Campbell, Size-dependent energy and adhesion of Pd nanoparticles on graphene on Ni(111) by Pd vapor adsorption calorimetry, ACS Catal. 13 (2023) 2670–2680.
[12] A.T. N'Diaye, T. Gerber, C. Busse, J. Mysliveček, J. Coraux, T. Michely, A versatile fabrication method for cluster superlattices, New J. Phys. 11 (2009) 103045.
[13] J. Knudsen, P.J. Feibelman, T. Gerber, E. Grånäs, K. Schulte, P. Stratmann, J.N. Andersen, T. Michely, Clusters binding to the graphene moiré on Ir(111): X-ray photoemission compared to density functional calculations, Phys. Rev. B 85 (2012) 035407.
[14] M. Petrović, P. Lazić, S. Runte, T. Michely, C. Busse, M. Kralj, Moiré-regulated self-assembly of cesium adatoms on epitaxial graphene, Phys. Rev. B 96 (2017) 085428.
[15] E. Vesselli, M. Peressi, Studies in Surface Science and Catalysis, vol. 177, Elsevier, Walthm, MA, USA, 2017, pp. 285–315.
[16] B. Wang, M.-L. Bocquet, Monolayer graphene and h-BN on metal substrates as versatile templates for metallic nanoclusters, J. Phys. Chem. Lett. 2 (2011) 2341–2345.
[17] M. Pivetta, S. Rusponi, H. Brune, Direct capture and electrostatic repulsion in the self-assembly of rare-earth atom superlattices on graphene, Phys. Rev. B 98 (2018) 115417.
[18] X. Liu, Y. Han, J.W. Evans, A.K. Engstfeld, R.J. Behm, M.C. Tringides, M. Hupalo, H.-Q. Lin, L. Huang, K.-M. Ho, D. Appy, P.A. Thiel, C.-Z. Wang, Growth morphology and properties of metals on graphene, Prog. Surf. Sci. 90 (2015) 397–443.
[19] F. Ruffino, F. Giannazzo, A review on metal nanoparticles nucleation and growth on/in graphene, Crystals 7 (2017) 219.
[20] J. Yang, K. Kim, Y. Lee, K. Kim, W.C. Lee, J. Park, Self-organized growth and self-assembly of nanostructures on 2D materials, FlatChem 5 (2017) 50–68.
[21] Z. Zou, V. Carnevali, M. Jugovac, L.L. Patera, A. Sala, M. Panighel, C. Cepek, G. Soldano, M.M. Mariscal, M. Peressi, G. Comelli, C. Africh, Graphene on nickel (100) micrograins: Modulating the interface interaction by extended moiré superstructures, Carbon 130 (2018) 441–447.
[22] Z. Zou, Unveiling the formation of graphene moiré patterns on fourfold-symmetric supports: Geometrical insight, J. Phys. Chem. C 125 (2021) 22705–22712.
[23] V. Carnevali, S. Marcantoni, M. Peressi, Moiré patterns generated by stacked 2D lattices: a general algorithm to identify primitive coincidence cells, Comput. Mater. Sci. 196 (2021) 110516.
[24] P. Giannozzi, et al., QUANTUM ESPRESSO: a modular and open-source software project for quantum, J. Phys.: Condens. Matter 21 (2009) 395502.
[25] P. Giannozzi, et al., Advanced capabilities for materials modelling with quantum ESPRESSO, J. Phys.: Condens. Matter 29 (2017) 465901.
[26] J.P. Perdew, K. Burke, M. Ernzerhof, Generalized gradient approximation made simple, Phys. Rev. Lett. 77 (1996) 3865–3868.
[27] S. Grimme, Semiempirical GGA-type density functional constructed with a long-range dispersion correction, J. Comput. Chem. 27 (2006) 1787–1799.
[28] F. Bianchini, L.L. Patera, M. Peressi, C. Africh, G. Comelli, Atomic scale identification of coexisting graphene structures on Ni(111), J. Phys. Chem. Lett. 5 (2014) 467–473.
[29] F. Mittendorfer, A. Garhofer, J. Redinger, J. Klimeš, J. Harl, G. Kresse, Graphene on Ni(111): Strong interaction and weak adsorption, Phys. Rev. Lett. B 84 (2011) 201401(R).
[30] D.C. Liu, J. Nocedal, On the limited memory BFGS method for large scale optimization, Math. Program. 45 (1989) 503–528.
[31] G. Henkelman, B.P. Uberuaga, H. Jónsson, A climbing image nudged elastic band method for finding saddle points and minimum energy paths, J. Chem. Phys. 113 (2000) 9901–9904.
[32] G. Henkelman, H. Jónsson, Improved tangent estimate in the nudged elastic band method for finding minimum energy paths and saddle points, J. Chem. Phys. 113 (2000) 9978–9985.
[33] A.H. Larsen, et al., The atomic simulation environment—a python library for working with atoms, J. Phys.: Condens. Matter 29 (2017) 273002.
[34] A. Kokalj, XCrySDen—a new program for displaying crystalline structures and electron densities, J. Mol. Graph. Model. 17 (1999) 176–179.
[35] D. Nečas, P. Klapetek, Gwyddion: an open-source software for SPM data analysis, Open Phys. 10 (2012) 181–188.
[36] D.W. Boukhvalov, M.I. Katsnelson, Enhancement of chemical activity in corrugated graphene, J. Phys. Chem. C 113 (2009) 14176–14178.
[37] H. Pan, Waved graphene: Unique structure for the adsorption of small molecules, Mater. Chem. Phys. 189 (2017) 111–117.
[38] S. Banerjee, A.M. Rappe, Mechanochemical molecular migration on graphene, J. Am. Chem. Soc. 144 (2022) 7181–7188.
[39] S. Banerjee, A.M. Rappe, Mechanochemical molecular motion using noncovalent interactions on graphene and its application to tailoring the adsorption energetics, ACS Mater. Lett. 5 (2023) 574–579.
[40] M. Imam, N. Stojić, N. Binggeli, First-principles investigation of a rippled graphene phase on Ir(001): The close link between periodicity, stability, and binding, J. Phys. Chem. C 118 (2014) 9514–9523.
[41] V. Tozzini, V. Pellegrini, Reversible hydrogen storage by controlled buckling of graphene layers, J. Phys. Chem. C 115 (2011) 25523–25528.
[42] O. Cretu, A.V. Krasheninnikov, J.A. Rodríguez-Manzo, L. Sun, R.M. Nieminen, F. Banhart, Migration and localization of metal atoms on strained graphene, Phys. Rev. Lett. 105 (2010) 196102.
[43] A. Sala, Z. Zou, V. Carnevali, M. Panighel, F. Genuzio, T.O. Menteş, A. Locatelli, C. Cepek, M. Peressi, G. Comelli, C. Africh, Quantum confinement in aligned zigzag pseudo-ribbons embedded in graphene on Ni(100), Adv. Funct. Mater. 32 (2022) 2105844.
[44] S. Stavrić, S. del Puppo, Ž. Šljivančanin, M. Peressi, First-principles study of nickel reactivity under two-dimensional cover: Ni_2C formation at rotated graphene/Ni(111) interface, Phys. Rev. Mater. 5 (2021) 014003.
[45] R.F.W. Bader, R.F.W. Bader, Atoms in Molecules, Oxford University Press, Oxford, England, UK, 1994.
[46] V. Chesnyak, S. Stavrić, M. Panighel, G. Comelli, M. Peressi, C. Africh, Carbide coating on nickel to enhance the stability of supported metal nanoclusters, Nanoscale 14 (2022) 3589–3598.
[47] K.T. Chan, J.B. Neaton, M.L. Cohen, First-principles study of metal adatom adsorption on graphene, Phys. Rev. B 77 (2008) 235430.
[48] H. Johll, H.C. Kang, E.S. Tok, Density functional theory study of Fe, Co, and Ni adatoms and dimers adsorbed on graphene, Phys. Rev. B 79 (2009) 245416.
[49] A.N. Rudenko, F.J. Keil, M.I. Katsnelson, A.I. Lichtenstein, Adsorption of cobalt on graphene: Electron correlation effects from a quantum chemical perspective, Phys. Rev. B 86 (2012) 075422.
[50] F. Ellinger, C. Franchini, V. Bellini, Magnetic *3d* adatoms on free-standing and Ni(111)-supported graphene, Phys. Rev. Mater. 5 (2021) 014406.

[51] N. Shahzad, J. Ren, C.K. Kim, DFT study on the interaction of subnanometer cobalt clusters with pristine/defective graphene, Bull. Korean Chem. Soc. 40 (2019) 446–452.
[52] S. Stavrić, M. Belić, Ž. Šljivančanin, Planar versus three-dimensional growth of metal nanostructures at graphene, Carbon 96 (2016) 216–222.
[53] Z. Zhou, F. Gao, D.W. Goodman, Deposition of metal clusters on single-layer graphene/Ru(0001): Factors that govern cluster growth, Surf. Sci. 604 (2010) L31–L38.
[54] M. Manadé, F. Viñes, F. Illas, Transition metal adatoms on graphene: A systematic density functional study, Carbon 95 (2015) 525–534.
[55] D.M. Eigler, E.K. Schweizer, Positioning single atoms with a scanning tunnelling microscope, Nature 344 (1990) 524–526.
[56] W. Ko, C. Ma, G.D. Nguyen, M. Kolmer, A.-P. Li, Atomic-scale manipulation and in situ characterization with scanning tunneling microscopy, Adv. Funct. Mater. 29 (2019) 1903770.
[57] T. Preis, S. Vrbica, J. Eroms, J. Repp, J.M. van Ruitenbeek, Current-induced one-dimensional diffusion of Co adatoms on graphene nanoribbons, Nano Lett. 21 (2021) 8794–8799.